J Math Imaging Vis (2012) 43:156–165
DOI 10.1007/s10851-011-0299-6

On the Use of Low-Pass Filters for Image Processing with Inverse Laplacian Models

Rehan Ali · Tunde Szilagyi · Mark Gooding · Martin Christlieb · Michael Brady

Published online: 25 May 2011

Abstract A novel signal processing-oriented approach to solving problems involving inverse Laplacians is introduced. The Monogenic Signal is a powerful method of computing the phase of discrete signals in image data, however it is typically used with band-pass filters in the capacity of a feature detector. Substituting low-pass filters allows the Monogenic Signal to produce approximate solutions to the inverse Laplacian, with the added benefit of tunability and the generation of three equivariant properties (namely local energy, local phase and local orientation), which allow the development of powerful numerical solutions for a new set of problems. These principles are applied here in the context of biological cell segmentation from brightfield microscopy image data. The Monogenic Signal approach is used to generate reduced noise solutions to the Transport of Intensity Equation for optical phase recovery, and the resulting local phase and local orientation terms are combined in an iterative level set approach to accurately segment cell boundaries. Potential applications of this approach are discussed with respect to other fields.

Keywords Inverse Laplacian · Monogenic signal · Transport of intensity · Low-pass filters · Microscopy image analysis

1 Introduction

Phase is a fundamental concept in both physics and signal processing. In the former, it describes the delay between two independent wave-based signals such as electromagnetic rays, string oscillations and other physical phenomena. In the latter, it contains information regarding signal shape, and can be related to wave-based phase through techniques such as the Fourier Transform. This paper describes a novel relationship between phase information from these different theoretical domains, and illustrates how this can be applied in a specific image processing context.

Our relationship specifically links *physical phase* from optical light propagation to *local phase* from signal feature detection. In this context, physical phase describes the perturbation of light caused by passing through a scattering object which has a different refractive index to the surrounding medium. A key equation describing this effect, the Transport of Intensity equation (TIE) [21], is frequently used to recover physical phase information from amplitude-only data. In contrast, local phase describes the shape or structure found in a specific signal region. Local phase cannot be calculated exactly due to limitations imposed by the Heisenberg Uncertainty Principle [13], but reasonable estimations can be obtained using band-pass quadrature filters. The Monogenic Signal is a powerful tool for multidimensional estimation of local phase, and is frequently used in signal processing [8].

R. Ali (✉)
Department of Radiation Physics, Stanford University, 875 Blake Wilbur Drive, CC-G206, Stanford, CA 94305, USA
e-mail: rsali@stanford.edu

T. Szilagyi · M. Brady
FRS FREng FMedSci Wolfson Medical Vision Lab, Department of Engineering Science, University of Oxford, Parks Road, Oxford OX1 3PJ, UK

M. Gooding
Mirada Medical Ltd, Innovation House, Mill Street, Oxford OX2 0JX, UK

M. Christlieb
Gray Institute for Radiation Oncology and Biology, University of Oxford, Old Road Campus Research Building, Oxford OX3 7QD, UK

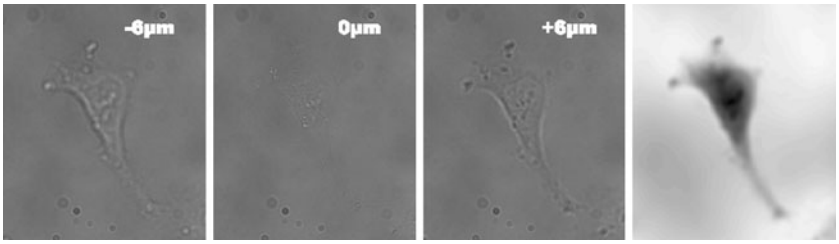

Fig. 1 A series of transillumination brightfield images of a live adherent HeLa cancer cell, at varying levels of focus. The *small dark circles* near the *top* and *bottom* are caused by oil-based artefacts on the lens. (*Right*) A TIE phase-recovered image acquired using the brightfield image defocus series, using our Matlab implementation of Eq. 3. Similar results were obtained using the implementation in the commercial Iatia QPM™ software

This paper shows that the TIE is equivalent to modifying a step in local phase estimation using the Monogenic Signal, where the band-pass filters are exchanged with low-pass filters. The use of low-pass filters in local phase estimation goes against accepted theory in this field, however doing so enables the powerful Monogenic Signal framework to be applied to a different class of problems. We present our results in cell microscopy image processing as an application of this relationship, and it is likely that others may exist. The next section provides the background to the TIE and Monogenic Signal, whilst Sect. 3 describes the relationships between the two. The context of our work is discussed in Sect. 4, along with possible connections with other research areas in computer vision.

2 Background

2.1 Physical Phase and the TIE

The problem of recovering phase information frequently occurs in many areas of applied physics (e.g. x-ray crystallography). It is typically solved indirectly using iterative solutions based on the Gerchberg-Saxton-Fienup (GSF) algorithm [9], however a direct solution can be obtained analytically in certain cases. One such case is in optical microscopy, where the TIE relates amplitude images from different focal planes to the underlying phase.

The TIE was derived by Teague in 1983 [21] from the Helmholtz Equation, the time-independent form of the Differential Wave Equation for a wave in empty space. The Helmholtz Equation is defined as

$$\left[\nabla^2 + \left(\frac{2\pi}{\lambda}\right)^2\right]\psi_z(x,y) = 0 \tag{1}$$

where λ is the wavelength and ψ_z is the component of the wave function perpendicular to the direction of motion (i.e. the object plane) at the focal distance Δz. Starting from Eq. 1, Teague derived the TIE,

$$\frac{2\pi}{\lambda}\frac{\partial}{\partial z}I = -\nabla \cdot I\nabla\phi \tag{2}$$

which relates the phase ϕ to the irradiance image I when $\Delta z = 0$, and the gradient of the irradiance in the z-axis. The TIE is an elliptical second-order PDE which Teague was able to reduce to the Poisson Equation by introducing an auxiliary variable. Teague also showed the solution to the TIE using Green's functions for the limited case of a circular object. The next significant advance was by Paganin and Nugent [19], who derived an algebraic solution for ϕ to the TIE:

$$\phi = -k\nabla^{-2}\left[\nabla \cdot \left(\frac{1}{I_0}\nabla\nabla^{-2}\frac{\partial I_0}{\partial z}\right)\right] \tag{3}$$

where $I \neq 0$ and ∇^{-2} represents an inverse Laplacian operator. Equation 3 can be solved using finite element methods [2] or Fourier Transform based approaches [23]. The latter is most commonly used because the Fast Fourier Transform (FFT) allows the solution to be computed very quickly. The FFT-based approach computes the inverse Laplacian by

$$\nabla^{-2}u(x,y) = \mathcal{F}^{-1}\left[\frac{\mathcal{F}[u(x,y)]}{|q|^2}\right] \tag{4}$$

where the spatial frequency vector, $q \neq 0$, is radially symmetric around the centre of the imaging field, and normal to the direction of propagation. Figure 1 demonstrates an example of phase recovery for a biological cell imaged using brightfield microscopy by solving the TIE.

2.2 Local Phase Estimation

Oppenheim and Lim demonstrated the importance of phase in images with a classic experiment in 1981 [17]. They switched around the phase and amplitude components of two distinct images, obtained through the Discrete Fourier Transform (DFT), and reconstituted the images using the inverse DFT to determine whether the amplitude or phase component had the greater influence on the final appearance. The resultant images turned out to resemble the images from which the phase component was derived. These early experiments studied image-based phase as a global property across the signal domain, however attention soon turned to

the properties of phase at a local level. Venkatesh and Owens showed that this local phase property, $\widetilde{\varphi}$, could be estimated using a pair of band-pass filters that are in quadrature, leading to the following definition:

$$\widetilde{\varphi}(t) = \arctan\left(\frac{b_o(t) \otimes f(t)}{b_e(t) \otimes f(t)}\right) \tag{5}$$

where b_e, b_o are even and odd band-pass quadrature filters, and $f(t)$ is the signal being analysed [22]. Typically, b_e is selected on the basis of the current application, and is used to derive b_o by applying the Hilbert Transform to b_e. Each filter responds maximally to the function with the same type of symmetry. Local phase is defined as the ratio of the responses of the quadrature filter pair to the band-passed signal, and as such, provides a measure of the oddness or evenness of the localised signal. This measure has the useful feature of being independent of signal amplitude due to a property called the *split of identity* which is assured by the analytic signal. The split of identity means that the representation is unique for a given signal and that the invariance-equivariance property is fulfilled. Invariance assures that certain transformations will not have an effect on the feature, i.e. local phase is invariant to changes in the local amplitude, and as such it is contrast and illumination independent. Equivariance on the other hand indicates that there is a clear monotonic dependency of the property extracted and the parameters of a transformation, for example, local phase's dependence on structures present in images [10].

The above theory is well established in fields such as electrical and acoustic signal processing, however it did not initially not lend itself to a simple extension to 2D signals as a suitable 2D odd filter did not appear to exist. The breakthrough came when Felsberg and Sommer showed that although 2D odd filters could not be defined using scalar-valued filters, the use of vector-valued filters could generate such a filter [8]. Felsberg and Sommer were able to determine this by using a 2D generalisation of the Hilbert Transform known as the Riesz Transform, and were thus able to generate 2D odd symmetric filters from a given even-symmetric band-pass filter by convolving it with the following odd frequency domain vector-valued filters:

$$\begin{aligned} H_1(u_1, u_2) &= j\frac{u_1}{\sqrt{u_1^2 + u_2^2}} \quad \text{and} \\ H_2(u_1, u_2) &= j\frac{u_2}{\sqrt{u_1^2 + u_2^2}} \end{aligned} \tag{6}$$

Their discovery led to a new representation of 2D signals known as the *Monogenic Signal*. They were able to derive expressions for local energy (an intensity-dependent measure of feature strength) and local phase using 2D spherical quadrature filters. In addition, a novel property was obtained, that of *local orientation*, which provides a measure of the direction of maximal signal variance. Given a suitable band-pass filtered image,

$$I_b(x, y) = I(x, y) \otimes b(x, y) \tag{7}$$

where $b(x, y)$ is the selected band-pass filter, the local energy ($\widetilde{A}$), local phase ($\widetilde{\varphi}$) and local orientation ($\widetilde{\theta}$) are given by

$$\widetilde{A}(x, y) = \sqrt{I_b^2 + (H_1 \otimes I_b)^2 + (H_2 \otimes I_b)^2} \tag{8}$$

$$\widetilde{\varphi}(x, y) = \arctan\left(\frac{H_2 \otimes I_b}{H_1 \otimes I_b}\right) \tag{9}$$

$$\widetilde{\theta}(x, y) = \arctan\left(\frac{I_b}{\sqrt{(H_1 \otimes I_b)^2 + (H_2 \otimes I_b)^2}}\right) \tag{10}$$

The computation of these is summarised in Fig. 2.

The choice of band-pass filter for calculating the odd and even quadrature filters is a key step, and has been discussed in a comprehensive review by Boukerroui et al. [5]. Boukerroui examined the properties of several families of band-pass filters, including Gabor, log-Gabor, Gaussian Derivative, Difference of Gaussian (DoG) and Cauchy filters, and

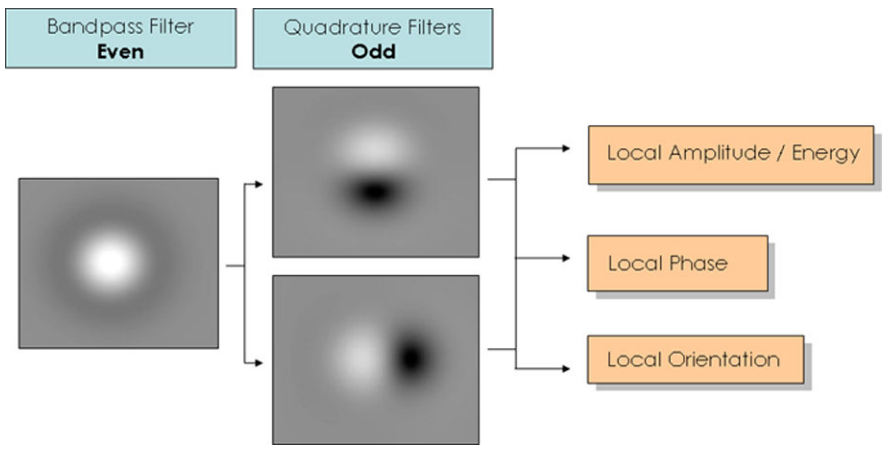

Fig. 2 The Monogenic Signal allows the derivation of local energy, local phase and local orientation for 2D signals. The images describe an even Difference of Gaussian filter and its corresponding odd quadrature filter pair

determined that with the exception of the Gabor filter, most were suitable for feature detection. In our experience, improved results can be obtained using a scale-invariant filter devised by Mellor and Brady [15]. This is a tunable filter which produces images with very sharp boundary edge features, which is described in further detail in Sect. 3.2.

3 Relating the TIE to the Monogenic Signal

Our specific application for local phase is the segmentation of biological cell boundaries from brightfield microscopy images. These images are commonly acquired from entry-level research microscopes which contain no hardware-based contrast enhancement. Biological cells are transparent fluid-filled objects which act as a lens. They appear near-invisible when the microscope is in-focus, but exhibit increased contrast when defocusing the microscope due to diffraction effects. The improvement in contrast is at the cost of image resolution, due to blurring by the microscope's Point Spread Function (PSF). One popular approach to segmenting cells in such images is to improve the contrast and then use simple image processing techniques. In 2002, Nugent et al. published a technique called Quantitative Phase Microscopy (QPM), which solved the TIE directly to recover the phase properties of the sample. The solution inside cells is of a different refractive index to the external medium, and thus a phase image provides improved contrast images where the cells can be clearly visualised [3]. An example result can be seen in Fig. 1. These images can then be easily thresholded, for example in [7].

One significant aspect of Fig. 1 is that the solution contains a low frequency field in the background. Volkov demonstrates that this is due to the application of inappropriate boundary conditions to the solution of Eq. 3, and recommends the use of periodic boundary conditions [23]. We found that the application of different boundary conditions did not significantly reduce the low frequency field in our images. The field becomes more significant for larger images with multiple cells and additional noise. Figure 3 shows the phase solution for larger images, where it is dominated by very strong low frequency noise which obscures the cells. This effect, which confounds any attempt to segment the cells on the basis of recovered phase, has been widely reported in the literature [4, 12, 18, 23], along with solutions to minimise it through experimental changes and image filtering, which have had limited success.

The Monogenic Signal provides a way to sidestep the effects of the low frequency noise, first by observing that a key step in the FFT-based solution for the TIE can be incorporated into the Monogenic Signal to produce results which resemble those from solving the TIE. It is then noted that the Mellor-Brady filter can be used to approximate these results, but with the added advantage of increased tunability. Finally, applying the modified Mellor-Brady filter with the Monogenic Signal framework results in local phase images with reduced levels of low-frequency noise, along with additional local amplitude and local orientation images which together provide a rich resource for more powerful image processing of brightfield image data.

3.1 The Monogenic Signal can Reproduce TIE Phase-Recovered Images

We start by noting that Eq. 4, the FFT-based solution for the inverse Laplacian calculated for solving the TIE, can be regarded as convolving the input image $\frac{\partial I}{\partial z}$ with a radially symmetric low-pass filter $q(x, y)^{-2}$, where q is the spatial frequency. This is identical to Eq. 7 of the Monogenic Signal formulation, with $I(x, y) \equiv \frac{\partial I}{\partial z}$ and $b(x, y) \equiv q^{-2}$. Local energy and local phase images were computed using a $\frac{\partial I}{\partial z}$ derivative image as the input for Eq. 7. The results in Fig. 4 show that when the derivative image is used as the input, the resulting local energy and local phase resemble the TIE recovered phase results shown in Fig. 3, thus demonstrating that the Monogenic Signal has the potential to reproduce TIE phase recovered images. In contrast, when the in-focus brightfield image is used as the input, the results are meaningless (data not shown). This demonstrates that the q^{-2} filter is only applicable to specific types of images.

The use of the TIE FFT filter to compute local energy and local phase suggests that the Monogenic Signal may have

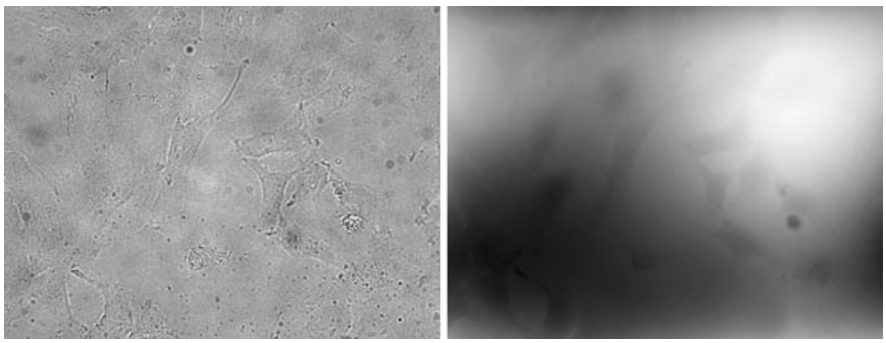

Fig. 3 (*Left*) A brightfield image of multiple adherent HeLa cancer cells. The image is slightly defocused for clarity. (*Right*) TIE phase-recovered image, displaying a large low frequency noise artefact

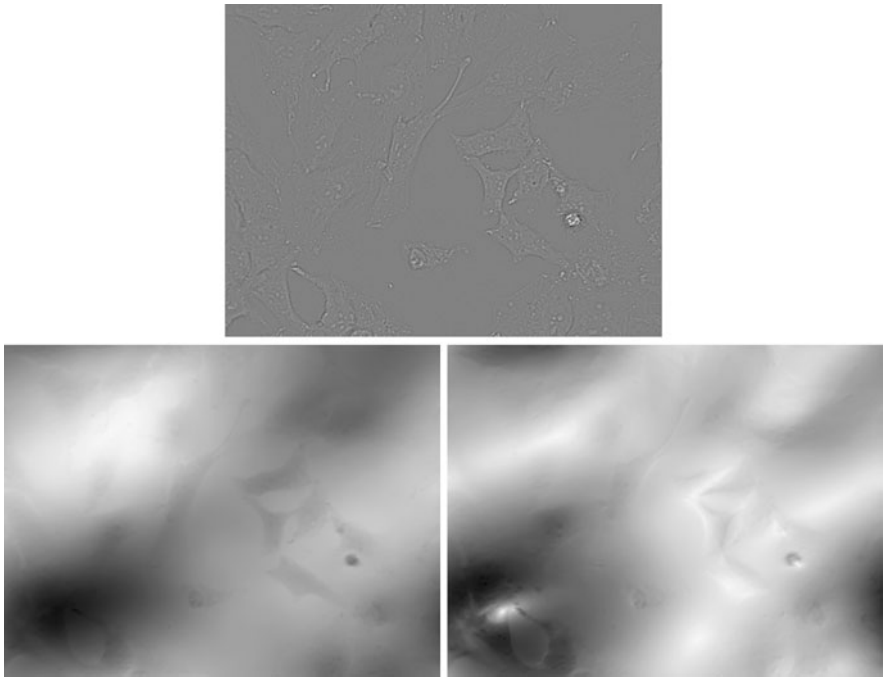

Fig. 4 (*Top*) An input derivative image $\frac{\partial I}{\partial z}$ for Eq. 7. (*Bottom*, *left-to-right*) The output local energy image and local phase image computed from the input derivative image, using the TIE-derived q^{-2} low-pass filter

potential uses other than as a feature detector. The results suggest that physical phase φ can be approximated by

$$\varphi \approx \nabla^{-2} \frac{\partial I}{\partial z} \tag{11}$$

Teague actually derived Eq. 11 from the TIE by introducing an auxiliary function ψ [21], using

$$\nabla \psi = I \nabla \phi \tag{12}$$

to give

$$\nabla^2 \psi = \frac{-2\pi}{\lambda} \frac{\partial I}{\partial z} \tag{13}$$

where ψ acts to scale the intensity values to produce physically meaningful values. The key point is that the use of low-pass filters to generate quadrature filter pairs can produce results within the Monogenic Signal framework which approximate the solution to the Poisson equation for phase recovery. This confers two potential advantages. The first is that if a filter can be found to approximate the q^{-2} low-pass filter, but which is also tunable, then it may be possible to 'dial out' the low frequency noise. The Mellor-Brady filter is such a filter, and its application is discussed in the next section. The second is that the Monogenic Signal permits computation of local amplitude, local phase and local orientation, which permit the development of advanced image processing algorithms.

3.2 The Mellor-Brady Filter can Approximate the TIE Low-Pass Filter

The choice of band-pass filter for calculating the odd and even quadrature filters is a key step when using the Monogenic Signal. Earlier, we introduced the Mellor-Brady filter. This useful filter is derived from the idea of geometric moments, $M_{p,q}$,

$$M_{p,q} = \int \int_{-\infty}^{\infty} I(x, y) x^p y^q \, dx \, dy \tag{14}$$

where p, q determine the order of the moments. Positive order geometric moments are often used to produce scale and rotation invariant global image metrics such as the centre of image intensity mass. Mellor used the definition for negative order moments to produce local measures, and combined this with negative powers of the radius $r(x, y) = \sqrt{x^2 + y^2}$ to make the measures rotationally invariant:

$$M_k(x, y) = \int \int I(x, y) r^{-k}(x - u, y - v) \, du \, dv \tag{15}$$

This is equivalent to convolution with a radially symmetric low-pass filter r^{-k}, which is undesirable for feature detection due to the existence of a DC component. A band-pass filter is created by taking the difference of two such filters to give the spatial domain filter

$$f(r) = \left[\frac{1}{r^{\alpha+\beta}} - \frac{1}{r^{\alpha-\beta}} \right] \tag{16}$$

where α and β are parameters which control the filter profile. In practice, the algorithm is used with parameter values

of $\alpha = 3.25$, $\beta = 0.25$, as this results in a band-pass filter which is relatively scale-invariant. However when $\alpha \to 0$, it becomes a low-pass filter whose properties are comparable to the q^{-2} filter. Figure 5 compares the Mellor-Brady filter frequency domain profile against the q^{-2} filter for several values of α. It can be seen that the case where $\alpha = 0.25$ displays a high degree of similarity to the q^{-2} filter.

The Mellor-Brady filter is used to compute the local energy, local orientation and local phase for the derivative image in Fig. 4. The results are shown in Fig. 6 using α values of $0.25, 1.5, 3.5$. At $\alpha = 3.5$ the local energy image shows very weak feature signals, which is expected given the low level of contrast of the original derivative image in Fig. 4. The local phase image highlights cellular anatomic features, which is expected given that local phase estimation using band-pass filters and the Monogenic Signal is an established intensity-invariant feature detection technique. As α decreases, the cell boundaries become emphasised in the local energy images, and the local orientation values point towards the cell boundaries from increasing distances. The cell interiors begin to fill in as α decreases, and at $\alpha = 0.25$ they approximate the TIE phase recovered images in Fig. 3. The low frequency noise patterns also begin to manifest themselves in the local phase images, and these are strongest for $\alpha = 0.25$. Significantly, in comparison to the TIE recovered phase image in Fig. 3, the low frequency noise component of the $\alpha = 0.25$ image is repressed and the edge features are significantly enhanced. This ability of the low-pass Mellor-Brady filter to generate output similar to the TIE approach, but to additionally control and tune the level of low-frequency noise, makes it potentially more suitable for cell segmentation purposes compared to the TIE phase-recovered images.

3.3 The Low-Pass Mellor-Brady Filter can Provide Additional Information

The information derived from the Monogenic Signal combined with the low-pass Mellor-Brady filter can facilitate the development of advanced image processing algorithms. Figure 7 shows the low-pass local phase and local orientation images obtained for a given brightfield image and its derivative image. In this case, the local phase image allows thresholding or region-growing algorithms to be applied to identify the cells. The local orientation image directs algorithms towards the cell boundary features, and thus can act as a driving force which allows the algorithm to escape from local minima. These have been incorporated into an automatic level-set framework for segmenting cell boundaries. Complete details of the segmentation algorithm are available at [1]. In brief, a multi-region level set implementation based on the framework by Sethian [20] is used. A signed

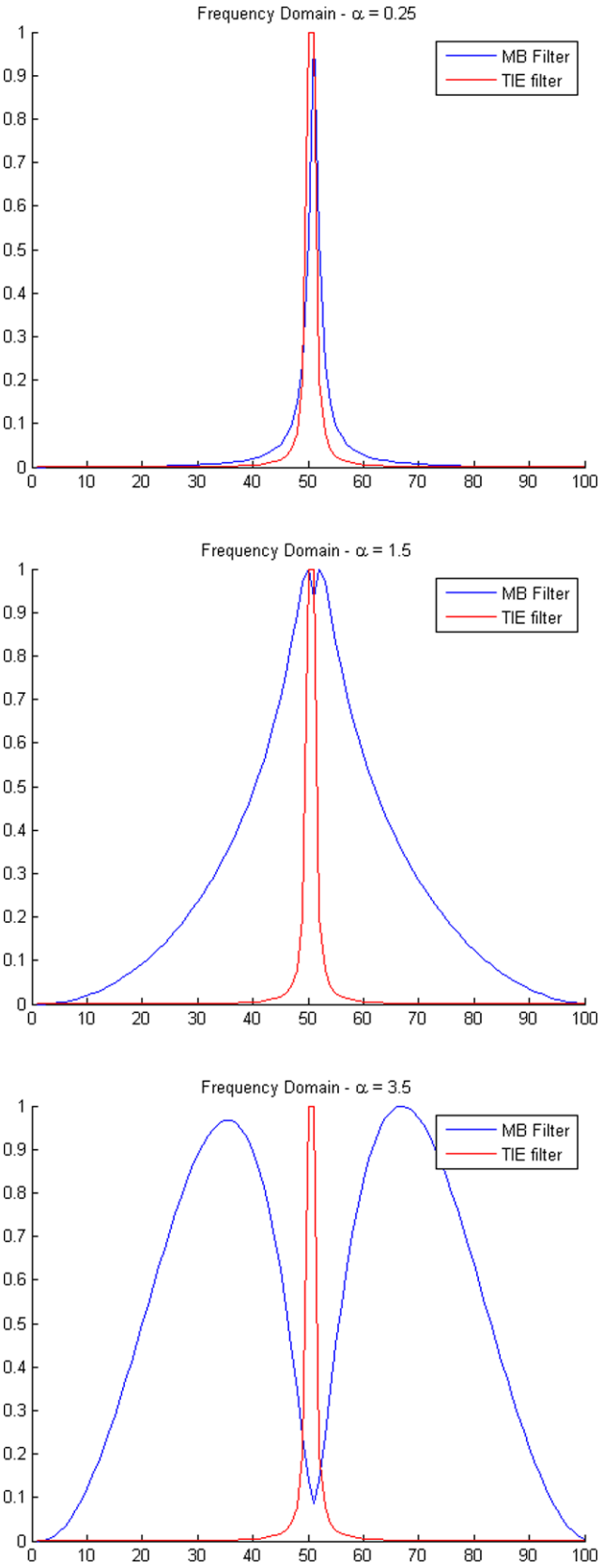

Fig. 5 (Colour online) Frequency domain plots of the Mellor-Brady filter profile (*blue*, Eq. 16) for $\alpha = 0.25, 1.5, 3.5$, compared to the TIE q^{-2} filter profile (*red*, based on Eq. 4)

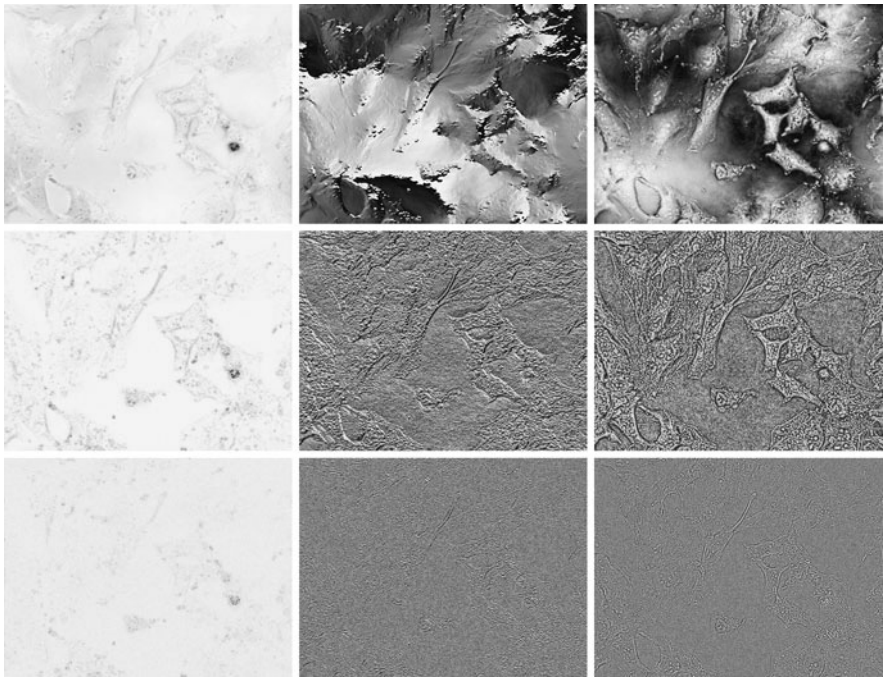

Fig. 6 (*Left to right column*) Local energy, local orientation and local phase images computed using the derivative image in Fig. 4, using the Mellor-Brady filter with values of $\alpha = 0.25$ (*top row*), $\alpha = 1.5$ (*middle row*) and $\alpha = 3.5$ (*bottom row*). Standard applications of the Monogenic Signal use a band-pass filter ($\alpha = 3.5$) for feature detection, however our application uses $\alpha = 0.25$, which yields a low-pass filter. Each column is rendered using the same colour scale (0–1 for local energy, $0–2\pi$ for local orientation and local phase)

distance function ϕ is generated, and the level set PDE below is solved to convergence:

$$\frac{\partial \phi}{\partial t} + F|\nabla \phi| = 0 \tag{17}$$

where the speed term F is given by

$$F = F_{\text{phase}} + F_{\text{orientation}} + F_{\text{smooth}} \tag{18}$$

The first two terms in Eq. 18 use local phase and local orientation images which have been computed using the Mellor-Brady low-pass filter ($\alpha = 0.25$, $\beta = 0.25$). F_{phase} is a region term computed over the local phase image, whilst $F_{\text{orientation}}$ uses the local orientation image to guide the level set evolution, by comparing it at each iteration to the direction of $\nabla(\phi = 0)$:

$$F_{\text{orientation}} = \cos(\theta_{\nabla\phi} - \theta_{LO}) \tag{19}$$

where $\theta_{\nabla\phi}$ is the angle of the normal vector of ϕ, and θ_{LO} is the local orientation angle at the corresponding pixel position. The third term, F_{smooth}, is a standard regularising term using the curvature of ϕ. Sample results of the segmentation algorithm are shown at the bottom of Fig. 7. The algorithm was able to correctly segment 81.3% (±3.2) of cell body pixels, and was able to produce results on 85% of cells tested. As a comparison, a Chan and Vese level set [6] was applied to the TIE phase recovered images, and was only able to segment 62% of cells with an accuracy of 76.1% (±2.1), due to the confounding influence of the strong low-frequency fields observed in Fig. 3.

In summary, the use of low-pass local phase images makes the algorithm considerably more robust, and slightly more accurate, than the TIE-based algorithm, due to the suppression of the low-frequency noise fields and the enhancement of the cell boundaries. The local orientation images confer an additional advantage by enabling the level set to converge faster on the optimal solution. This example illustrates one way in which the use of low-pass Monogenic Signal filters can provide an advantage for specific applications.

3.4 Analysis of the Low-Pass Mellor-Brady Filter

In Sect. 2.1 the TIE equation was introduced as Eq. 4 by solving the inverse Laplacian. Given the theory of Monogenic Signal computation in 2D (Fig. 2), one could observe that the first step in the process is the application of a band-pass filter. In this section it is shown that a careful choice of the filter, with specific attention given to the filter's characteristics in the spatial domain, holds significant potential for applications involving the solution to inverse Laplacians.

The band-pass filter defines the nature of the features to be extracted from digital images. Typically filter properties are assessed in the frequency domain, with one of the most important being the selection of narrow frequency bands which then assures a proper recovery of the phase properties. However, it is often neglected that, for local feature extraction such as phase properties, the localization requirement in the spatial domain is equally (or more) vital.

One way of summarizing filter properties for local feature definition was presented in [16]. There are three desired

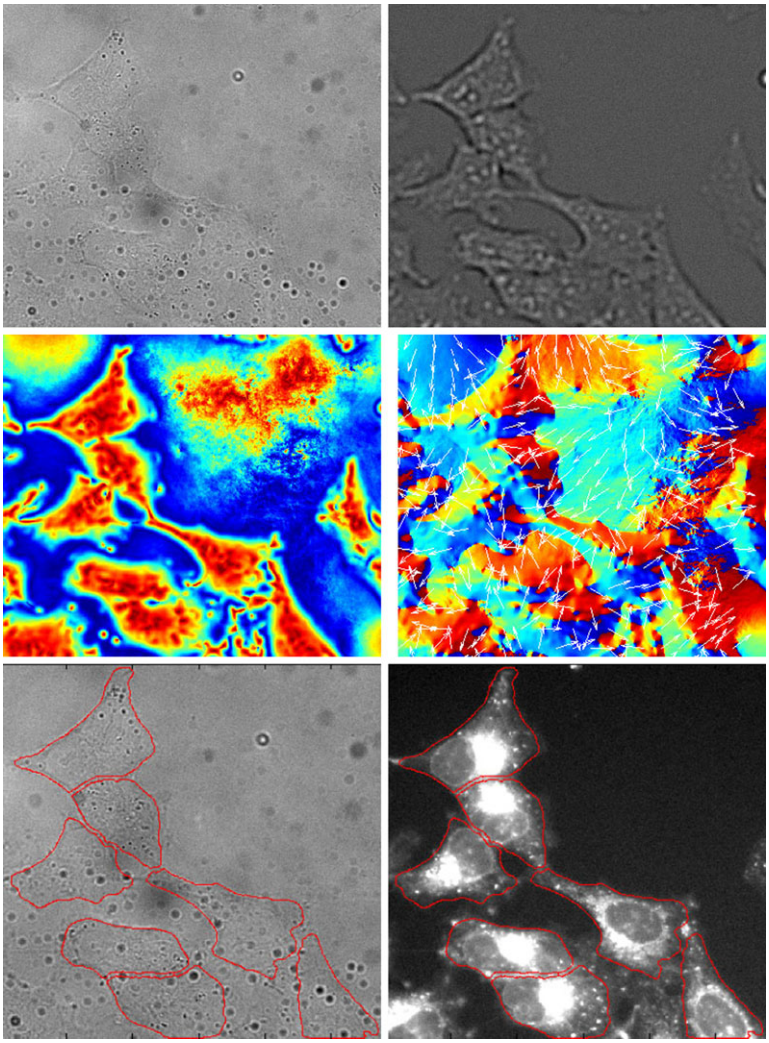

Fig. 7 (Colour online) (*Top-left*) In-focus brightfield image, (*top-right*) derivative image, (*middle-left*) local phase map using low-pass filter, (*middle-right*) local orientation map using low-pass filter (with directional arrows superimposed). The scale in the local phase and local orientation images is $-\pi$ (*blue*) to $+\pi$ (*red*). (*Bottom row*) Cell boundary segmentation results superimposed on brightfield and fluorescent images. The local phase and local orientation images were generated by applying the low-pass Mellor-Brady filter ($\alpha = 0.25, \beta = 0.25$) to the derivative image, as discussed in Sect. 3.2

properties suggested as guidelines:

1. Scale invariance

$$f(ar) = s(a)f(r), \quad \text{where } s(a) \neq 0, \forall a \neq 0 \tag{20}$$

2. Strong criteria of energy localisation of isotropic filters in the spatial domain

$$\int_0^R 2\pi r f(r)^2\,dr \geq \int_R^\infty 2\pi r f(r)^2\,dr, \quad \forall\ R > 0, R \in \mathbb{R} \tag{21}$$

   This means that the energy deposited in a finite area (a circle for isotropic filters) is much greater than any energy that is left outside this area, i.e. at a distance greater than the finite radius R.
3. The mean value of the filter is 0 in the spatial domain, i.e. the filter DC value is 0, which allows accurate gradient estimation and is also essential for phase estimation because of the ratio of the even and odd filters that are needed.

Notice that the localisation is given as a strong criteria, which is not definitely necessary in real applications. Therefore, we hereby define a weaker condition of energy deposition namely

$$\int_0^R f(r)^2\,dr \geq \int_R^\infty f(r)^2\,dr, \quad \forall\ R > 0, R \in \mathbb{R} \tag{22}$$

This means that we are only looking for the filter magnitude without the area term. As a result it is no longer required that the infinite area of the filter support is counterbalanced by the infinitely small filter values in the region $[R, +\infty)$, $\forall R \in \mathbb{R}$ finite number. It can be derived from the above definitions that if a filter has the localisation property according to the strong criteria then the weak criteria also holds, however the converse is not true, hence the naming convention introduced in this paper.

First we turn our attention to the filter that is used by the TIE approximation, $F(q) = \frac{1}{q^2}$ for which the spatial equivalent is defined as $-\sqrt{\frac{\pi}{2}}x\text{Sign}(x)$, where $\text{Sign}(x) =$

$-1, \forall x < 0$, and $+1$ otherwise. To verify its spatial localisation properties, the integral formula for the strong criterion is computed to be

$$\int r \cdot f(r)^2 \, dr = c_1 \cdot r^4, \tag{23}$$

where $c_1 \in \mathbb{R}$ is constant. The weak criterion readily available to be $c_2 \cdot r^3$, with $c_2 \in \mathbb{R}$ constant. This shows that neither the spatial localisation in the strong nor in the weak sense can be satisfied (Eqs. 21 and 22).

In contrast, the Mellor-Brady filter satisfies all three conditions suggested for any $\alpha < -1$, as demonstrated in [16]. In order to mimic the TIE filter, the Mellor-Brady filter parameters are set to $\alpha = \beta = 0.25$ (Sect. 3.2). In this scenario, all the above properties hold, with the strong localisation being replaced by the weak one, as in Eq. 22.

4 Conclusions

This paper describes how the use of low-pass filters with the Monogenic Signal framework can provide a novel way to address problems which require numerical solutions to the inverse Laplacian. The use of low-pass filters with the Monogenic Signal is unusual because prior work in this area is based almost exclusively on the use of band-pass filters. In cases where a non-zero DC component exists, for example with the Gabor filter, steps are often taken to correct this [5]. In our case however, the use of a tunable low-pass filter produces results that facilitate the solution to a problem in microscopy image processing. This demonstrates the potential utility of non-standard filters when used to estimate local feature metrics using the Monogenic Signal.

The key features of our approach are twofold. Firstly, it introduces the ability to use tunable filters to mimic the $\frac{1}{|q|^2}$ term in the fourier transform solution to the inverse Laplacian, such as the one used to solve the TIE (Eq. 4), whilst controlling the degree of low-frequency noise introduced into the solution (by satisfying the localisation criterion, unlike the q^{-2} TIE-based filter). Secondly, it uses the split of identity feature of the Monogenic Signal to derive three equivariant properties, namely local energy, local phase and local orientation. We have shown these representations to be valuable in the context of an iterative level set algorithm which segments the boundary of biological cells from brightfield microscopy image data, however the principles are likely to be generalisable to other problem domains involving inverse Laplacians and image-based numerical solutions.

There are several example applications requiring inverse Laplacians. First, the Marr-Poggio theory of early vision envisaged the construction of a primal sketch in which zero crossing contours were computed from a series of octave separated Laplacian of a Gaussian filters (i.e. the Laplacian of a Gaussian was convolved with the image). A central claim of their work was that the original image can be reconstructed from the zero crossing contours, and this is done by solving the inverse problem [14]. In a similar vein, Horn proposed a theory based around the human perceptual ability known as lightness. Horn realised that lighting varies slowly, however the associated colour changes (or more precisely, albedo changes) are sharp, and he solved for lightness using the greens function for the inverse Laplacian [11]. These suggest that, at least in the domain of computer vision, further applications of our method may exist.

Acknowledgements The authors would like to thank Nathan Cahill, Niranjan Joshi and Christopher Yau for constructive discussions. R.S. and T.S. were funded by the Life Sciences Interface Doctoral Training Centre (LSI DTC) and the Engineering and Physical Sciences Research Council (EPSRC).

References

1. Ali, R., Gooding, M., Christlieb, M., Brady, M.: Automatic segmentation of adherent biological cell boundaries and nuclei from brightfield microscopy images, Machine Vision and Applications, April 2011, online publication http://www.springerlink.com/content/6158882w07024402/
2. Barbero, S., Thibos, L.: Error analysis and correction in wavefront reconstruction from the transport-of-intensity equation. Opt. Eng. **45**, 1–6 (2006)
3. Barone-Nugent, E., Barty, A., Nugent, K.: Quantitative phase-amplitude microscopy I. Optical microscopy. J. Microsc. **206**, 194–203 (2002)
4. Bellegia, M., Schofield, M., Volkov, V., Zhu, Z.: On the transport of intensity technique for phase retrieval. Ultramicroscopy **102**(1), 37–49 (2004)
5. Boukerroui, D., Noble, A., Brady, M.: On the choice of Band-Pass quadrature filters. J. Math. Imaging Vis. **21**, 53–80 (2004)
6. Chan, T., Vese, L.: Active contours without edges. IEEE Trans. Image Process. **10**(2), 266–277 (2001)
7. Curl, C., Harris, T., Harris, P., Allman, B., Bellair, C., Stewart, A., Delbridge, L.: Quantitative phase microscopy: a new tool for measurement of cell culture growth and confluency in situ. Eur. J. Physiol. **448**, 462–468 (2004)
8. Felsberg, M., Sommer, G.: The monogenic signal. IEEE Trans. Signal Process. **49**(12), 3136–3144 (2001)
9. Fienup, J.: Phase retrieval algorithms: a comparison. Appl. Opt. **21**, 2758–2769 (1982)
10. Granlund, G., Knutsson, H.: Signal Processing for Computer Vision. Springer/Kluwer Academic, Berlin (1995)
11. Horn, B.: Robot Vision. MIT Press, Cambridge (1986)
12. Ishizuka, K., Allman, B.: Phase measurement of atomic resolution image using transport of intensity equation. J. Elect. Microscopy **54**, 191–197 (2005)
13. Mallat, S.: A Wavelet Tour of Signal Processing. Academic Press, San Diego (1998)
14. Marr, D.: Vision—A Computational Investigation into the Human Representation and Processing of Visual Information. Freeman, New York (1982)
15. Mellor, M., Brady, M.: Phase mutual information as a similarity measure for registration. Med. Image Anal. **9**(4), 330–43 (2005)
16. Mellor, M., Hong, B.-W., Brady, M.: Locally rotation, contrast, and scale invariant descriptors for texture analysis. IEEE Trans. Pattern Anal. Mach. Intell. **30**(1), 52–61 (2008)

17. Oppenheim, A., Lim, J.: The importance of phase in signals. Proc. IEEE **69**, 529–550 (1981)
18. Paganin, D., Barty, A., McMahon, P., Nugent, K.: Quantitative phase-amplitude microscopy. III. The effects of noise. J. Microsc. **214**, 51–61 (2004)
19. Paganin, D., Nugent, K.: Noninterferometric phase imaging with partially coherent light. Phys. Rev. Lett. **80**(12), 2586–2589 (1998)
20. Sethian, J.: Level Set Methods and Fast Marching Methods. Cambridge University Press, Cambridge (1999)
21. Teague, M.: Deterministic phase retrieval: a Green's function solution. J. Opt. Soc. Am. **73**, 1434–1441 (1983)
22. Venkatesh, S., Owens, R.: On the classification of image features. Pattern Recognit. Lett. **11**, 339–349 (1990)
23. Volkov, V., Zhu, Y., De Graef, M.: A new symmetrized solution for phase retrieval using the transport of intensity equation. Micron **33**(5), 411–416 (2002)